Low-temperature water–hydrogen-molecule collisions probed by pressure broadening and line shift

Brian Drouin[1] and Laurent Wiesenfeld[2]

[1]*Jet Propulsion Laboratory, California Institute of Technology, Pasadena, California 91109-8099, USA*

[2]*UJF-Grenoble 1/CNRS, Institut de Planétologie et d'Astrophysique de Grenoble (IPAG) UMR 5274, Grenoble F-38041, France*

(Received 22 February 2012; revised manuscript received 18 May 2012; published 7 August 2012)

Theoretical H_2O-H_2 pressure broadening and line shifts are compared with experimental values for three water rotational transitions. These transitions, which occur at terahertz frequencies, are primary radiant coolants for collapsing interstellar clouds that contain water. They are observed by the submillimeter/FIR Herschel space observatory. Systematic effects in previous pressure-broadening measurements that were due to ortho-hydrogen to para-hydrogen conversion have been overcome, and the present results follow the expected behavior predicted by collision theory. The systemic error, discovered through comparisons between theory and experiments, is due to conversion of ortho hydrogen to para hydrogen by water ice below 40 K. This process occurs on a time scale very short compared to astrophysical processes and may be pertinent to ice-grain interactions in the interstellar medium.

DOI: 10.1103/PhysRevA.86.022705 PACS number(s): 34.20.−b, 34.50.Ez, 95.30.Ky, 95.85.Fm

I. INTRODUCTION

Determining the relative density of water in its various isotopic forms with respect to molecular hydrogen in interstellar matter depends crucially on the quenching rate of the rotational levels of water by molecular hydrogen [1]. These quenching rates vary considerably with the spin state of H_2. Quenching rates of H_2O by para H_2 (pH_2) with angular momentum restricted to $j = 0$ are often 1 order of magnitude less effective than quenching by H_2 with angular momentum $j > 0$ and, in particular, by ortho H_2 (oH_2) ($j = 1$) [2,3]. The goal of this effort is to precisely measure the respective roles of $j = 0$ and $j > 0$ molecular hydrogen in the quenching and line-broadening processes by means of a careful experimental setup and comparison with a large-scale theoretical simulation. We monitor the pressure-broadening and pressure-shift cross sections while controlling the spin state of H_2, which alternates between para $I_{\rm tot} = I_{\rm H} + I_{\rm H'} = 0$ and ortho $I_{\rm tot} = 1$ with rotational angular momenta $j = 0,1,2,\ldots$. We set up a comparison between theoretical predictions and experimental observations for the main terahertz (THz) transitions of both ortho and para $H_2{}^{16}O$ water, which are observed by the Herschel space observatory [4].

In this more detailed and carefully designed theoretical and experimental version, we will put special emphasis on the role of the spin conversion of H_2, from oH_2, to pH_2. This topic has been experimentally studied in some recent papers, with discussion emphasizing the role of O_2 impurities in amorphous water [5–7]. The oH_2 to pH_2 abundance ratio (OPR) of nascent H_2 on amorphous water has been measured at temperatures of importance for astrophysics [8]. All these papers, alongside many astrophysical models [9,10], strongly emphasize the necessity for modeling of the oH_2 to pH_2 conversion. The interplay of careful spectroscopic experiments and theoretical quantum computation provides new aspects on the H_2-H_2O interaction.

This paper is organized as follows: We describe in detail the experimental setup and results (Sec. II), the theoretical computations (Sec. III), and we finish with a discussion and conclusion (Sec. IV).

II. EXPERIMENT

Measuring the evolution of pressure broadening of water (or CO) by collisional cooling [11–13] with the ambient gas H_2 at a lower temperature reproduces reasonably well the conditions prevailing in many interstellar gases. A cryogenic gas apparatus designed for the injection of condensable gases and subsequent cooling of the injected gas to the bath temperature is utilized to measure spectroscopic properties of gases below their gas condensation temperatures. While the buffer gas pressure remains constant, the flowing gas condenses on the cell walls and is probed spectroscopically during its random walk through the buffer gas.

Previous measurements on hydrogen buffer gases exhibited strong departures from predicted collisional broadening at the lowest temperatures measured. Furthermore, a systematic bias in the gas temperature (compared to the cell temperature) was identified for the water-broadening dataset [13]. The systematic temperature bias was hypothesized to be due to direct heating of the gas by the warm injector needle, which must be maintained above 300 K for continuous water flow. In the previous paper, this injector protruded 3 cm into the buffer gas to reach an area 1 cm above the radiation path. For the present paper, a shroud was built to extend the cold cell walls down around the injector, leaving only 1 mm of hot metal inside the cold gas. Doppler width measurements of the 556-GHz water absorption feature confirmed a 1:1 correspondence of the gas and cell temperatures over the entire range of cell temperatures (20–250 K). Therefore, in the present paper, the cell temperature is taken as the gas temperature.

Krupnov [14] suggested the previously observed temperature dependence of the water-hydrogen broadening [13] may be due to preferential adsorption (cf. Ref. [15]) of the oH_2 component of the buffer gas into the amorphous water ice that forms continuously on the apparatus walls. This implies that the OPR may not be stable during the experiment and might explain the observed reductions in broadening since pH_2 is a much weaker broadening gas. With no magnetic materials in the cell, the prior paper had assumed the OPR to be stable at the normal hydrogen (nH_2) value of 3.

To test Krupnov's hypothesis, experiments were performed with a variety of new conditions. First, a pH_2 generator was built, and broadening measurements for both nH_2 and pH_2 were performed across the temperature range, utilizing the same procedures as before. The results for nH_2 above 40 K were entirely consistent with previous papers. However, upon closer examination, below 40 K, evidence of ortho-to-para conversion (OPC) of hydrogen became apparent. This is not entirely unexpected since water ice has been shown, at lower temperatures, to adsorb molecular hydrogen (not necessarily preferentially) and (internally) to convert the H_2 to the $j = 0$ (para) rotational level [16,17]. However, at these temperatures, temperature programed desorption (rather than thermal balance) was required to return the converted hydrogen to the gas phase. Also very recent experiments, available just after our previous series of experiments, confirm the OPC at 15 K (this paper also suggests that nascent molecular hydrogen, formed by recombination of H atoms in amorphous water ice, is initially statistical with an OPR of 3) [8]. Furthermore, below 28 K, preferential adsorption (as suggested by Krupnov) was also observable. Both effects were highly dependent on the water flow rate as well as the amount of time water had flowed (i.e., the ice deposition rate and ice thickness). The effects of these two processes were discerned from time-dependent differences in the water-hydrogen broadening as well as time dependence of the system pressure. With rapid water flow rates, the hydrogen gas pressure was observed to decrease linearly with time at temperatures below 28 K, and this was accompanied by an exponential decay of the pressure-broadened linewidth, which asymptotically approached values slightly higher than measured in purified pH_2. This OPC thermalization was slow, occurring on time scales of minutes, however, the initial OPR change, upon injection of nH_2 was rapid, presumably because the preferential adsorption proceeds rapidly in the ice that has been under vacuum, and further adsorption occurs more slowly at a rate proportional to the flow rate as fresh ice is collected.

Improvements in the optics for the THz beam enabled detection of the water absorptions at smaller concentrations than in previous papers. This enabled slower flow rates to be employed, flow rates which resulted in much thinner ice. Furthermore, the system was regularly warmed to room temperature and was evacuated until low water vapor pressures were attained (cleaned). The reduced flow and minimal ice layer slowed the OPC rates (to hours), and the OPR could be stabilized at or near the nH_2 value. However, the preferential adsorption still occurred (to varying degrees) upon introduction of nH_2 to the system. To verify stability of the OPR, measurements were performed through successive additions of nH_2, followed by measurements performed between extractions of the same buffer gas in similar steps. The nH_2 (OPR = 3) measurements above 28 K were considered viable for the present dataset only if these two measurements agreed within the experimental precision. If the pressure broadening between the two series was different, the system was cleaned prior to any further measurements.

At the lowest temperatures ($T < 28$ K), the adsorption effect was mitigated through addition of an excess of nH_2, typically 2 orders of magnitude more than needed for the measurement. This excess gas rapidly fills the available pores in the amorphous water ice, and the OPR changes slightly. Typically, the pressure reading stabilized at a value 1%–10% lower than the initial pressure. Immediately after this step, the pressure was reduced to the desired pressure for the measurement. The pressure broadening was then measured by repeating this process for different pressures. Unlike the data above 28 K, this procedure precludes the OPC stability test and must be considered a lower bound since the OPR may indeed be smaller than 3.

Before describing the new results in detail, it is pertinent to describe the physics of the gas-ice interaction elucidated by the new procedure through comparison with the older data taken in an icy system. Figure 1 shows data from Dick *et al.* [13] (plotted vs T_{cell}) as gray triangles which *had* been assumed to have OPR = 3. Clearly the new data, which are believed to have OPRs of 3 (black circles) and 0 (green triangles), bracket the former dataset, which straddles the two OPR extremes at high and low temperatures. The solid black line is calculated as a H_2O-H_2 pressure-broadening cross section for *thermalized* H_2, using the experimental parameters reported later that fit our new data. If the system contained sufficient amounts of a fast ortho-to-para converter, one would expect the data to always follow the *thermalized* H_2 value (black line). Even though our new procedure demonstrates that the ice content is variable across the range for efficient conversion, they do not indicate strict adherence to efficient thermal conversion (notice the deviation between the gray data points and the black line). The new results do indicate that data reported in Dick *et al.* [13] were affected by the interaction with the large amounts of high-density amorphous ice in the system. Unfortunately, there are several temperature-dependent processes occurring in the system (1) OPC, (2) an amorphous water-ice phase change, and (3) H_2 adsorption. Amorphous water ice is in a low-density form above 68 K, below 68 K, it slowly transitions to a high-density form. Below 38 K, it is completely the high-density amorphous water ice [18]. Since all of the hydrogen adsorption and desorption studies have been

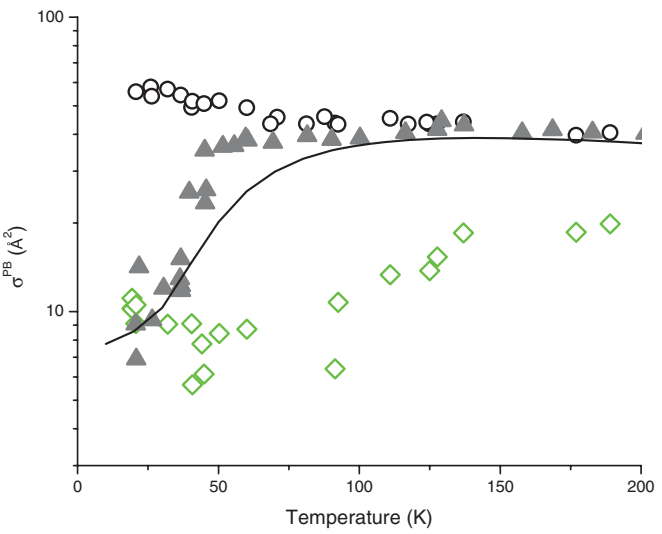

FIG. 1. (Color online) Pressure-broadening cross sections for $J_{K_aK_c}$: 1_{11}-0_{00} water in hydrogen with uncontrolled OPR shown as filled gray triangles [13], black circles: OPR = 3 and green diamonds: OPR = 0.

performed below this transition temperature, the observed adsorption and conversion effects are attributed to the high-density form of amorphous water ice. It is not clear whether the low-density form has any interaction with molecular hydrogen. All three of these phenomena occur within the temperature range at which the OPR changes most rapidly for thermalized molecular hydrogen in an icy environment. The only definitive statement that can be made through comparison of the thermal curve and previous (icy) data in Fig. 1 is that, above 40 K, the conversion and/or adsorption processes are not efficient.

The evidence for adsorption at the lowest temperatures indicates that the residence time of the molecular hydrogen within the ice lattice is also increased as the temperature is lowered. Adsorption and desorption experiments have shown that the emergent OPR of molecular hydrogen depends strongly on residence time in the solid phase. Indeed, it is during this time that the $j = 1$ hydrogen molecules may come into close contact with large dipolar field gradients in the vicinity of water monomers in the lattice. With the present dataset, it is impossible to disentangle these different phenomena, and it certainly appears, from inspection of Fig. 1, that the effect is not just a simple temperature-dependent thermalization of the OPR. Temperature- and time-dependent experiments are possible, and these may distinguish between the preferential adsorption and the conversion mechanisms.

Despite the fascinating effects of low-temperature water ice on molecular hydrogen, the premise put forth in Dick *et al.* [13] remained open—How well do calculated collisional cross sections reproduce the experimental pressure-broadening data? The current effort, initiated following Krupnov's quick response [14] to the last experiments [13], has enabled a new dataset that is largely free from ice contamination. Furthermore, the new dataset is more robust, containing data with OPRs of both 3 and 0 as well as pressure-shift cross sections. This has enabled us to extend comparisons with the theoretical model to higher precision and has increased confidence in both experimental and theoretical results.

Utilizing the new procedures, a dataset of three water rotational transition pressure- broadening cross sections $\sigma^{\rm PB}(T)$ and pressure-shift cross sections $\delta^{\rm PS}(T)$ for both nH_2 and pH_2 has been collected in the temperature range of 20–250 K. The experimental values of pressure broadening and pressure shifts for pH_2 and nH_2 were determined via linear regression of the pressure-dependent differential linewidth or differential line-shift measurements determined from a deconvolution method [19] utilizing pairs of separate spectral scans. The natural spectral units (MHz/Torr) of the linewidth and line shift were converted to the units of cross sections ($Å^2$) via

$$\phi(T) = 0.447\sqrt{T/\mu}\,\Delta\nu/\Delta p, \tag{1}$$

where $\Delta\nu$ is the Lorentzian half width at half maximum [for $\phi(T) = \sigma^{\rm PB}(T)$] or frequency shift [for $\phi(T) = \delta^{\rm PS}(T)$].

III. THEORY

In response to the concerns raised by the previous measurements [13], we have re-calculated the pressure-broadening cross sections utilizing the best available potential-energy surfaces (PESs) for H_2O-H_2 [20,21]. These previous papers reported broadening cross sections for two fundamental rotational transitions (levels of H_2O are usually denoted as $J_{K_aK_c}$): 0_{00}-1_{11} (para H_2O) and 1_{01}-1_{10} (ortho H_2O). Here, we extend this effort, both to include the transition 1_{11}-2_{02} and to include pressure-shift computations. To the best of the authors knowledge, this is the first computation of pressure shifts and comparisons with experiments, for a system of such a low symmetry [22]. Let us recall the pressure-broadening and ordinary cross-sectional formulas as put forward in Ref. [21]. J is the partial-wave total angular momentum, j_1, τ_1 are the water asymmetric rotor quantum numbers, j is the H_2 rotational quantum number, and α represents all collision specific angular quantum numbers (recoupling and orbital angular momenta) with unprimed quantities before collision and primed quantities after collision,

$$\begin{aligned}\phi^{\rm PB}(j_1'\tau_1'j' \leftarrow j_1\tau_1 j; E) &= \frac{\pi}{k^2}\frac{1}{2j+1}\sum_{JJ'\alpha\alpha'\bar{\alpha}\alpha'} X(J,J',j_1,j_1',j,j',\alpha,\bar{\alpha},\alpha',\bar{\alpha}') \\ &\times \langle j_1\tau_1 j\alpha|\mathbf{T}^J(E)|j_1\tau_1 j\bar{\alpha}\rangle\langle j_1'\tau_1' j'\alpha'|\mathbf{T}^{J'}(E')|j_1'\tau_1' j'\bar{\alpha}'\rangle^\star,\end{aligned} \tag{2}$$

and

$$\sigma(j_1'\tau_1'j' \leftarrow j_1\tau_1 j; E) = \frac{\pi}{k^2}\frac{1}{(2j_1+1)(2j+1)}\sum_{J\alpha\alpha'}(2J+1) \times |\langle j_1'\tau_1' j'\alpha'|\mathbf{T}^J(E_t)|j_1\tau_1 j\alpha\rangle|^2. \tag{3}$$

In Eqs. (2) and (3), $\mathbf{T}^J(E) = 1 - \mathbf{S}^J(E)$ is the transition matrix at partial-wave total angular momentum J. The $X(\cdot)$ function groups all angular coupling coefficients and parity terms. E_t, E, and E' are the *total* energies, corresponding to the kinetic energy $(\hbar k)^2/2\mu$, μ being the collision reduced mass, and $\hbar k$ being the momentum. Note that, for $\phi^{\rm PB}$, the $\mathbf{T}$-matrix elements are for *elastic*-scattering amplitudes, whereas, for inelastic scattering, the matrix elements are *inelastic*-scattering amplitudes.

The real part of $\phi^{\rm PB}$ yields $\sigma^{\rm PB}$, the pressure-broadening cross section. It is related to the total inelastic cross sections (summed over all initial and final states) and to a difference of elastic amplitudes by means of the optical theorem [23]. The imaginary part $\delta^{\rm PS}$, the pressure shift, cannot be simplified. Its computation is particularly sensitive to all details of both the PES and the convergence of the sum in Eq. (2). Indeed, it originates from a difference in the accumulated phase of the scattering amplitudes in the two elastic channels. Its computation is very time consuming, and reliability is not easily reached. Note also that it can be positive or negative, depending on the sign of the phase differences.

Those formulas have been used by summing the $\mathbf{S}$-matrix elements provided by the quantum computations, performed by the MOLSCAT scattering code [24]. The MOLSCAT code was executed on the large clusters of the CIMENT Network [25], with 6 to 12 cores in parallel, thanks to the OpenMP recoding of MOLSCAT [24].

Energy of the levels were taken at $E_{\rm rot} = 23.799\,48\,(1_{01})$, $37.153\,84\,(1_{11})$, $42.402\,40\,(1_{10})$, and $70.132\,88\,(2_{02})$ $\rm cm^{-1}$. For a given collision relative kinetic energy E_k, the pressure-broadening cross sections $\sigma^{\rm PB}(E_k)$ and the pressure-shift cross sections $\delta^{\rm PS}(E_k)$ are determined. For the temperature

dependence of these quantities, calculation of the Maxwellian distribution of collision energies for each temperature must utilize a large enough basis to follow all the resonances.

This basis contains finer energy steps $\Delta E_k = 0.2$ up to 0.5 cm^{-1} for $E_k \leqslant 200\ \text{cm}^{-1}$ and results in higher precision for the temperature-dependent cross sections. Also, we did *not* rely on the convergence of the usual $\sigma_{\text{inelastic}}(E_k)$ to stop the summation in partial waves. Rather, we imposed angular momentum of water J to go up to $J = 8$ up to $E_k = 80\ \text{cm}^{-1}$ and $J = 10$ afterwards. Also, we summed partial waves up to $J^{\text{total}} = 55$ by imposing very strict convergence of the σ_{elastic} at the level of less than 1%. We checked that values converged for both pressure broadening and pressure shifts. The basis set was capped at $E_{\text{rot}}(H_2O) < 1500\ \text{cm}^{-1}$ for all transitions. The pH_2 basis set was taken at $j = 0,2$ throughout the computation. Results of any close-coupling computations involving pH_2 have been shown repeatedly to crucially need that the $j = 2$ pH_2 levels be included in the basis [21,26,27]. All included, for each E_k, ten separate runs of close-coupling calculations were performed since the pressure-broadening and pressure-shift computations rely on **S** matrices taken at the same kinetic energy for all different channels involved, including those with varying $j(H_2)$.

IV. RESULTS AND DISCUSSION

Pressure broadening, pressure shift, and elastic and inelastic cross sections are each given as a function of E_k in Fig. 2. The scale of energy is the collision (kinetic) energy, hence, it is different for each of the cross sections depicted. Pressure broadening and pressure shifts, averaged over a Maxwellian distribution of E_k at temperatures $20\ \text{K} \leqslant T \leqslant 250\ \text{K}$ are given in Fig. 3 for comparison with experimental values.

The usual resonance pattern is present for the $\sigma(E_k)$, and is particularly prominent for collisions with pH_2, both for elastic and inelastic scatterings as well as for pressure broadening and pressure shifts. Resonances are much less present for collisions with oH_2 as has been noticed previously because of the interference of many partial waves at varying total angular momentum J for one single partial wave. However, the detailed resonance structures of $\sigma(E_k)$ and of $\sigma^{\text{PB}}(E_k)$ are not fully parallel (even if they are computed from exactly the same set of **S** matrices). We may relate that to the very structure of the sections: The kinetic energies being the same for the incoming (say 1_{11}) and outgoing (say 2_{02}) waves, the total energy is different for the two **T**-matrix brackets composing the pressure-broadening scattering probability, one being equal to E_t in Eq. (3) and the other not.

The magnitudes of the elastic and inelastic cross sections show that neither of the two contributions to $\sigma^{\text{PB}}(E_k)$, the inelastic nor the interference of elastic amplitudes [23], could be neglected, at least, in the resonance region. The complex detailed resonance structure of $\delta^{\text{PS}}(E_k)$ for both oH_2 and pH_2 collisions underlines even more the necessity of very precise computation of the scattering amplitudes that interfere to give rise to the effects calculated here.

For each water transition, over 40 experimental data points (see symbols Fig. 3) or 30 theoretical data points were utilized in least-squares analyses to determine coefficients of the power-law expressions in Eq. (4), see Supplemental

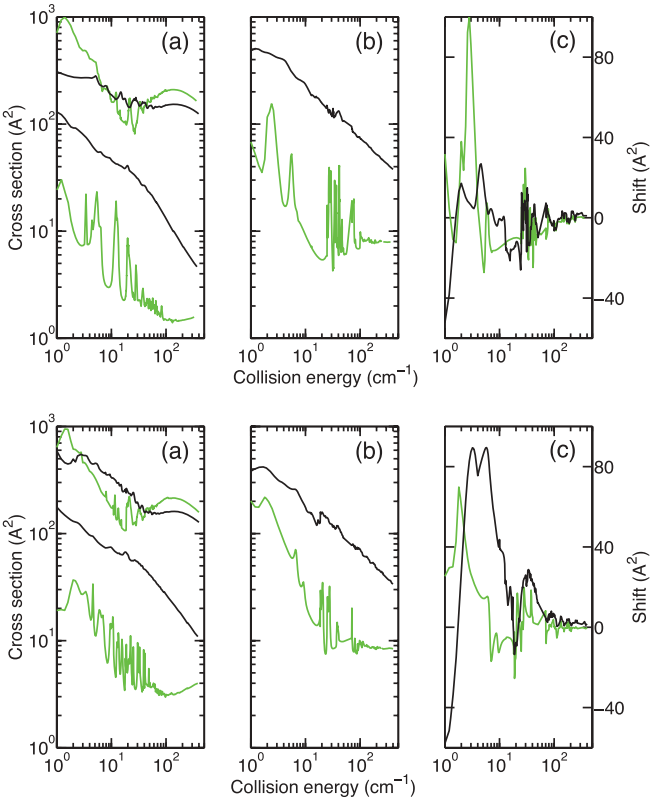

FIG. 2. (Color online) Upper three panels: cross sections, computed for the para-H_2O transition 1_{11}-2_{02} and lower three panels: the ortho-H_2O transition 1_{01}-1_{10}. All panels: black lines: collision with oH_2, $j, j' = 1$; green lines: collisions with pH_2, $j, j' = 0$. Panels (a), upper two sections: elastic 1_{11} or 1_{01} and inelastic excitation cross sections. Panels (b), pressure-broadening cross sections. Panels (c), pressure-shift cross sections.

Material [28]. Two parameters for each state are considered, a reference value [$\phi_0 = \sigma_0^{\text{PB}}(j)$ or $\delta_0^{\text{PS}}(j)$] at a given temperature and a temperature exponent. The reference temperature was chosen at $T_0 = 20$ K,

$$\phi(T) = \sum_{j=0,1,2} f_j \phi_0 (T/T_0)^{n_j}. \tag{4}$$

The coefficient f_j represents the fractional state population for hydrogen. For theoretical data models, this value was fixed to unity for the calculated hydrogen colliding state and zero for all other states. For the experimental data and for the theoretical curves plotted in Fig. 3, the fractions are $f_1 = 0.75$ for nH_2 or $f_1 = 0$ for pH_2 (the f_3 component of nH_2 is negligible for this temperature range and precision), and f_0 and f_2 fractions were calculated at each temperature utilizing Boltzmann statistics.

Although a minor fraction, the $j = 2$ rotational state contributes to broadening parameters above 100 K. Without $j = 2$, the nH_2 and pH_2 experimental datasets would be independent, and $j = 1$ parameters could be calculated from fitting of the nH_2 and pH_2 data directly to effective power laws. However, the non-negligible fraction of $j = 2$ in nH_2 would introduce systematic errors, such as an underestimation of the $j = 1$ temperature dependence. Furthermore, some independent information on the broadening of $j = 2$ is clearly present in the purified pH_2 dataset, which shows minima

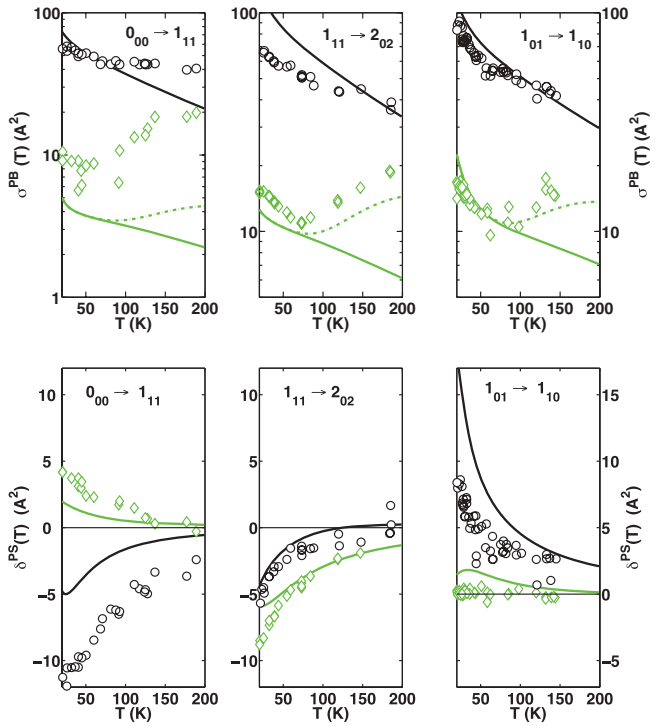

FIG. 3. (Color online) Upper panels: pressure broadening and lower panels: pressure shifts as a function of temperature for the indicated transitions. Lines, theory [via Eq. (1)]. Symbols: experiment. Green lines and diamond symbols: pH_2. Black lines and circular symbols: nH_2. See text for details. Note the different y scales for the various panels.

near 75 K—curvature that cannot be addressed with a single power law. The thermalized state populations for the $j = 0, 2$ levels enable these minima to be described by two separate monotonic decreasing functions. We observed that the power-law parameter n_2 of the $j = 2$ level was generally correlated with the n_1 parameter and only marginally improved the fit statistics. Furthermore, the values could be fixed to the $j = 1$ values without changing the $j = 1$ values significantly, so this was performed for the fits. Both values of the shift power-law expression for $j = 2$ were similarly fixed to $j = 1$ values.

The resulting expressions are given in Table I for the pressure-broadening cross sections and in Table II for the pressure-shift cross sections. These expressions (and the Boltzmann statistics for $j = 0,1,2,3$ H_2) were utilized for the calculation of the thermalized hydrogen curve in Fig. 1. Values obtained for $j = 0$ were consistent with values obtained from direct analysis of the pH_2 data below 75 K, and values obtained for $j = 1,2$ were consistent with a $j = 1$ value derived from that value and an aggregate value from a direct fit of the nH_2 data.

We display theoretical curves calculated under experimental conditions (Fig. 3) as well as the modeled power-law expressions in the $j = 0, 1, 2$ basis (Tables I and II) for comparison. For pH_2, the black solid line is for pH_2, $j = 0$, (but with the full $j = 0,2$ basis). The dashed-dotted line is constructed by adding a contribution from pH_2, $j = 2$. Since computational burden prevented a full calculation, the $j = 2$

TABLE I. Theoretical and experimental pressure-broadening collision cross sections of hydrogen with water. Expressions are given for units of Å^2. Theoretical values are fitted to calculated values between 20 and 82 K. The shaded rows contain values fitted to experimental data, and unshaded rows are values fitted to the theoretical data.

$J'_{Ka'Kc'}$ -J_{KaKc}	$\sigma^{PB}(T)$-H_2 ($j = 0$)		$\sigma^{PB}(T)$-H_2 ($j = 1$)	
1_{01}-1_{10}[a]	21.6	$(T/20)^{-0.56}$	125.6	$(T/20)^{-0.464}$
	16.9(2)	$(T/20)^{-0.30(3)}$	110.1(13)	$(T/20)^{-0.36(1)}$
1_{11}-0_{00}[a]	4.82	$(T/20)^{-0.269}$	84.5	$(T/20)^{-0.404}$
	8.5(8)	$(T/20)^{+0.13(8)}$	80(2)	$(T/20)^{-0.24(2)}$
2_{02}-1_{11}[a]	12.52	$(T/20)^{-0.202}$	144.3	$(T/20)^{-0.490}$
	14.9(5)	$(T/20)^{-0.20(3)}$	99(2)	$(T/20)^{-0.35(1)}$

[a]The variable n_2 was fixed to the corresponding value of n_1 for each transition. Values for $\sigma_0^{PB}(j = 2)$ determined from the experimental data are 138(10), 84(8), and 114(5) for the 1_{01}-1_{10}, 1_{11}-0_{00}, and 2_{02}-1_{11} transitions, respectively.

contribution was extrapolated from the $\sigma_{inelastic}$ values' ratios in that range of energies. We implicitly assume thereby that, at the higher energies, the σ^{PB} is dominated by the inelastic behavior. Similar numbers would be computed if we assumed $\sigma^{PB}_{j=1}(E) \sim \sigma^{PB}_{j=2}(E)$.

Both experimental and theoretical cross-sectional data have several general features: (1) The high-temperature values for the three different water transitions all converge to similar values for nH_2 and pH_2 separately, (2) at the lowest temperatures, for pH_2, the cross section of the 1_{11}-0_{00} (the pH_2O ground state) transition departs from the other two transitions, and (3) at the lowest temperatures, for nH_2, all three transitions exhibit unique behavior, with the pH_2O ground state having the smallest cross section.

For the two transitions 1_{11}-2_{02} and 1_{01}-1_{10}, the agreement between experiment and theory for the pressure broadenings and pressure-shift cross sections is outstanding (within 30% nearly everywhere), both in interaction with $j = 0$ and $j = 1$. Less favorable agreement is found for $j = 0$ collisions and the 0_{00}-1_{11} transition (40%–80%). The $j = 1$ interaction

TABLE II. Theoretical and experimental pressure-shift cross sections of normal and para hydrogen with water. Expressions are given for units of Å^2. Theoretical values are fitted to calculated values between 20 and 82 K. The shaded rows contain values fitted to experimental data, and unshaded rows are values fitted to the theoretical data.

$J'_{Ka'Kc'}$ -J_{KaKc}	$\delta^{PS}(T)$-H_2 ($j = 0$)		$\delta^{PS}(T)$-H_2 ($j = 1$)	
1_{01}-1_{10}[a]	1.86	$(T/20)^{-0.27}$	18.7	$(T/20)^{-0.83}$
	−0.09(5)	$(T/20)^{+0.3(4)}$	11.0(3)	$(T/20)^{-0.61(3)}$
1_{11}-0_{00}[a]	2.09	$(T/20)^{-0.73}$	−6.49	$(T/20)^{-0.71}$
	4.8(2)	$(T/20)^{-0.69(5)}$	−25.3(13)	$(T/20)^{-0.79(3)}$
2_{02}-1_{11}[a]	−6.44	$(T/20)^{-0.35}$	−4.71	$(T/20)^{-1.14}$
	−10.9(8)	$(T/20)^{-0.91(6)}$	−7.4(70)	$(T/20)^{-2.4(18)}$

[a]The variables $\delta_0^{PS}(j = 2)$ and n_2 were fixed to the corresponding values of δ_1 and n_1 for each transition.

with these levels exhibits nearly perfect agreement at low temperatures but diverges to 50% disagreement near 200 K. Given both the delicacy of measurements and the very difficult characterization of convergence of the theoretical computation, one could not expect better agreement. In particular, for both pressure shifts and pressure broadening, the magnitude of the theoretical prediction depends crucially on the difference in magnitude and phase between the *elastic S*-matrix elements $\langle i|S|i\rangle$ and $\langle f|S|f\rangle$, that is, on the difference in both magnitude and accumulated phase for the incoming ($|i\rangle$) and outgoing waves ($|f\rangle$) for two states at the same kinetic energy. Broadening with the lowest state transition 0_{00} is generally not as well reproduced by theory, plausibly because a different part of the potential is probed by the elastic S matrix connecting the isotropic 0_{00} state, especially so in the very-long-range part.

These intercomparisons provide valuable insight into the validity of the H_2O-H_2 PES in regions that are far from well-tested regimes. Indeed, even if the thermal equilibrium of the collisional cooling or pressure-broadening technique precludes direct measurements of collision energies, measurements of pressure-broadening and pressure-shift cross sections are highly useful as *absolute metrics*, which are not typically attained in collisional scattering techniques [26,29].

ACKNOWLEDGMENTS

Portions of this research were carried out at the Jet Propulsion Laboratory, California Institute of Technology, under contract with the National Aeronautics and Space Administration. L.W. thanks the French space agency CNES for travel support.

[1] A. Coutens, C. Vastel, E. Caux, C. Ceccarelli, S. Bottinelli, L. Wiesenfeld, A. Faure, Y. Scribano, and C. Kahane, Astron. Astrophys. **539**, A132 (2012).
[2] A. Faure, N. Crimier, C. Ceccarelli, P. Valiron, L. Wiesenfeld, and M.-L. Dubernet, Astron. Astrophys. **472**, 1029 (2007).
[3] F. Daniel, M.-L. Dubernet, and A. Grosjean, Astron. Astrophys. **536**, A76 (2011).
[4] E. F. van Dishoeck, L. E. Kristensen, A. O. Benz, E. A. Bergin, P. Caselli, J. Cernicharo, F. Herpin, M. R. Hogerheijde, D. Johnstone, R. Liseau, B. Nisini, R. Shipman, M. Tafalla, F. van der Tak, F. Wyrowski, Y. Aikawa, R. Bachiller, A. Baudry, M. Benedettini, P. Bjerkeli, G. A. Blake, S. Bontemps, J. Braine, C. Brinch, S. Bruderer, L. Chavarría, C. Codella, F. Daniel, T. de Graauw, E. Deul, A. M. di Giorgio, C. Dominik, S. D. Doty, M. L. Dubernet, P. Encrenaz, H. Feuchtgruber, M. Fich, W. Frieswijk, A. Fuente, T. Giannini, J. R. Goicoechea, F. P. Helmich, G. J. Herczeg, T. Jacq, J. K. Jørgensen, A. Karska, M. J. Kaufman, E. Keto, B. Larsson, B. Lefloch, D. Lis, M. Marseille, C. McCoey, G. Melnick, D. Neufeld, M. Olberg, L. Pagani, O. Panić, B. Parise, J. C. Pearson, R. Plume, C. Risacher, D. Salter, J. Santiago-García, P. Saraceno, P. Stäuber, T. A. van Kempen, R. Visser, S. Viti, M. Walmsley, S. F. Wampfler, and U. A. Yıldız, Publ. Astron. Soc. Pac. **123**, 138 (2011).
[5] M. Chehrouri, J.-H. Fillion, H. Chaabouni, H. Mokrane, E. Congiu, F. Dulieu, E. Matar, X. Michaut, and J. L. Lemaire, PhysChemChemPhys. **13**, 2172 (2011).
[6] L. Amiaud, J. H. Fillion, S. Baouche, F. Dulieu, A. Momeni, and J. L. Lemaire, J. Chem. Phys. **124**, 094702 (2006).
[7] V. Shevtsov, A. Scherbakov, P. Malmi, E. Ylinen, and M. Punkkinen, J. Low Temp. Phys. **104**, 211 (1996).
[8] N. Watanabe, Y. Kimura, A. Kouchi, T. Chigai, T. Hama, and V. Pirronello, Astrophys. J. Lett. **714**, L233 (2010).
[9] L. Pagani, E. Roueff, and P. Lesaffre, Astrophys. J. Lett. **739**, L35 (2011).
[10] N. Troscompt, A. Faure, S. Maret, C. Ceccarelli, P. Hily-Blant, and L. Wiesenfeld, Astron. Astrophys. **506**, 1243 (2009).
[11] M. J. Dick, B. J. Drouin, and J. C. Pearson, J. Quant. Spectrosc. Radiat. Transf. **110**, 619 (2009).
[12] M. J. Dick, B. J. Drouin, T. J. Crawford, and J. C. Pearson, J. Quant. Spectrosc. Radiat. Transf. **110**, 628 (2009).
[13] M. J. Dick, B. J. Drouin, and J. C. Pearson, Phys. Rev. A **81**, 022706 (2010).
[14] A. F. Krupnov, Phys. Rev. A **82**, 036703 (2010).
[15] V. Buch and J. P. Devlin, J. Chem. Phys. **98**, 4195 (1993).
[16] L. Amiaud, F. Dulieu, J.-H. Fillion, A. Momeni, and J. L. Lemaire, J. Chem. Phys. **127**, 144709 (2007).
[17] L. Amiaud, A. Momeni, F. Dulieu, J.-H. Fillion, E. Matar, and J.-L. Lemaire, Phys. Rev. Lett. **100**, 056101 (2008).
[18] P. Jenniskens and D. Blake, Science **265**, 753 (1994).
[19] H. Pickett, Appl. Opt. **19**, 2745 (1980).
[20] P. Valiron, M. Wernli, A. Faure, L. Wiesenfeld, C. Rist, S. Kedžuch, and J. Noga, J. Chem. Phys. **129**, 134306 (2008).
[21] L. Wiesenfeld and A. Faure, Phys. Rev. A **82**, 040702(R) (2010).
[22] F. Thibault, E. P. Fuller, K. A. Grabow, J. L. Hardwick, C. I. Marcus, D. Marston, L. A. Robertson, E. N. Senning, M. C. Stoffel, and R. S. Wiser, J. Mol. Spectrosc. **256**, 17 (2009).
[23] M. Baranger, Phys. Rev. **112**, 855 (1958).
[24] J. M. Hutson and S. Green, MOLSCAT computer code version 14, distributed by Collaborative Computational Project No. 6 of the Engineering and Physical Sciences Research Council, UK, 1994.
[25] https://ciment.ujf-grenoble.fr/cigri
[26] C.-H. Yang, G. Sarma, D. H. Parker, J. J. ter Meulen, and L. Wiesenfeld, J. Chem. Phys. **134**, 204308 (2011).
[27] M. Dubernet, F. Daniel, A. Grosjean, and C. Y. Lin, Astron. Astrophys. **497**, 911 (2009).
[28] See Supplemental Material at http://link.aps.org/supplemental/10.1103/PhysRevA.86.022705 for data points.
[29] C.-H. Yang, G. Sarma, J. J. ter Meulen, D. H. Parker, G. C. McBane, L. Wiesenfeld, A. Faure, Y. Scribano, and N. Feautrier, J. Chem. Phys. **133**, 131103 (2010).